Energy Equip. Sys. / Vol. 9/No. 3/Sep. 2021/ 229-248

ENERGY EQUIPSYS

Energy Equipment and Systems

http://energyequipsys.ut.ac.ir
www.energyequipsys.com

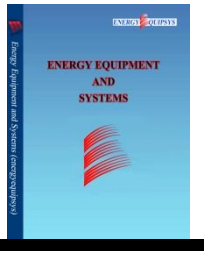

Cogeneration of power and hydrogen using Scamjet cooling system :Energy and exergy analyses

Authors

Hadi Ghaebi [a*]
Pouria Seyedmatin [a]

[a] Department of Mechanical Engineering, Faculty of Engineering, Mohaghegh Ardabili University, P.O.Box 179, Ardabil, Iran

Article history:

Received : 28 November 2020
Accepted : 23 May 2021

ABSTRACT

In the current study, a new integrated system is provided to prevent waste energy and reduce power consumption. This system consists of a cascade refrigeration system (for cooling) and an Organic Rankine cycle(ORC) (for power generation). These two cycles are combined through a heat exchanger. In fact, this heat exchanger acts as a condenser for the cascade refrigeration cycle and evaporator for ORC. The waste heat of the cascade refrigeration cycle is used to handle the ORC. In this way, a part of the power consumption of the cascade refrigeration cycle is satisfied by ORC. Thermodynamic simulation of the proposed system is carried out via Engineering Equation Solver(EES) software. A parametric study is done to evaluate the effects of the operational parameters on the performance of the integrated system. In addition, different working fluids are used in cascade refrigeration and ORC cycles. The results showed that by using the working fluids of R245fa, R717, and R141b in order in the low-temperature refrigeration cycle, high-temperature refrigeration cycle and ORC, one can produce cooling at -50 ° C and also reduce the power consumption up to 48.69% in the cascade refrigeration cycle.

Keywords: Thermodynamic Analysis, Scramjet, Hydrogen, Multi-Expansion, M-OCC, PEM Electrolyzer.

1. Introduction

The interest in airbreathing propulsion vehicles has been traced back many decades ago. To get more applicable access to propulsive devices due to their ability to uphold high-speed atmospheric flight, supersonic combustion ramjets (scramjets) have been proposed to be studied [1, 3]. The thermal management of the scramjet is considered a key issue in scramjet technology challenges due to the high heat release level in the scramjet combustion chamber. the heat flux density of scramjet is ranged between 0.5 and 2.5 MW per unit area for wall temperature of 500-2000 K at flight much number of 8. In such high temperature, not only the conventional known materials but also the most developed composite substances could not endure and operate properly [3]. Using fuel as the coolant in regenerative cooling systems has also been commonly regarded as one of the most common and feasible solutions for the scramjet cooling systems [4]. By this method, the heat absorption capacity of the fuel is utilized to cool the scramjet earlier than entering the combustion chamber. But, limited heat absorption capacity and fuel aboard can't supply the whole cooling needs of the scramjet adequately. In hydrogen-fuelled scramjets, the flow rate of fuel coolant will exceed the stoichiometric flow rate during the flight at a speed above a certain Mach number [8]. In other words, more fuel than the mission requisite

* Corresponding author: Hadi Ghaebi
Department of Mechanical Engineering, Faculty of Engineering, Mohaghegh Ardabili University, P.O.Box 179, Ardabil, Iran
Email: hghaebi@uma.ac.ir

should be conveyed by the scramjet due to the low heat sink of the fuel [5, 6]. Extra fuel onboard and its accessories increase the size and weight of the vehicle which noticeably decreases the performance of the vehicle [7]. The above-mentioned reasons entailed the necessity of increasing the heat sink capacity of fuel. Accordingly, Qin et al. [8] advanced the open cooling cycle (OCC) of scramjet engines as a scientifically feasible solution of increasing fuel heat sink without accretion in fuel flow rate. In their system, the high-temperature output coolant of the first cooling passage cools down in order to reuse it in the second cooling process. To decline the temperature of the coolant a turbine is installed to produce the power as well. This process can be repeated in several times that is called multi-OCC (M-OCC). In this scenario, the heat absorption capacity of the fuel is successively used; thus the required flow rate of the fuel (as coolant) will be reduced. OCC is also applicable to both hydrocarbon and hydrogen-fuelled scramjet engines. As well as M-OCC provides good opportunity to get the most optimum privilege of recovering waste energies in scramjet.The ancillary set-ups, including fuel injection, circuit measuring, and tracking controller systems on aircrafts and aerospace vehicles require a great deal of electrical power. Thus, for such a high speed enormous vehicles it is noticeably significant to provide an energy recovery set-up to address its surplus power needs [9]. In recent years, recovering energy for producing power and other required commodities has been utilized in numerous energy conversion systems. Co-production systems are introduced as the most efficient and pragmatic solutions for energy recovery purposes when low-quality heat resources (such as waste heat) are pondered [10]. Using co-production systems render the feasibility of producing other useful forms of energies such as heating, cooling, purified water and hydrogen alongside the power production [11-13]. Co-production (also known as Co-generation) systems have higher energy efficiency and low exergy destruction than the single-production systems under a same condition, as shown by Onovwiona and Ugursl [14]. Balta et al. [15] carried out a thermodynamic study of a high degree system electrolysis (HDSE) for cogeneration of H_2 and power, including a solar tower, a Brayton system, a Rankine system, and an organic Rankine system. In the electric generation segment, the total efficiencies are reported as 24.79% and 22.36% for energy and exergy, sequentially and in H_2 production section, the total efficiencies are obtained 87% and 88% correspondingly. Furthermore, H_2 production rate of the coupled cycle is calculated 0.057 kg/s with 1.98 kWh electricity consumption in a condition that the PEM temperature is 500 K. Ghaebi et al [16] has proposed two novel combined cycles for electricity and H_2 co-production utilizing a huge amount of wasted energy of the city gas post (CGP) regulators in which the high-pressure NG is reduced to a suitable pressure for consumption. These two systems are integrated by a combination of a CGP system and a Rankine system (RS) as well as an absorption power system (APS) as an alternative power system. In both systems, PEM electrolyzer is used to produce hydrogen. The power sub-cycle is actuated by the waste heat of CGP and PEM is operated by a fair segment of net output electricity. An executive and comparative 4E (energy, exergy, economy and environment) analysis of both systems have been fulfilled. The results of the analysis have shown 6.868 kg/h and 6.351 kg/h hydrogen production as well as 8.571 MW and 7.618 MW power production for the CGP-RS and CGP-APS systems, respectively. The exergy destruction study has demonstrated that the generator of the system has been introduced as the highest exergy destructive component (in both systems). Li and Wang [17] have presented a theoretical model of producing power from the waste heat of scramjet. In their study, a thermoelectrical generator (TEG) is assimilated with a regenerative cooling cycle of a scramjet engine for power production. The results of this study revealed power production of 61.69 kW and exergy efficiency of about 22% for a fuel flow rate of 0.4 kg/s. And a parametric analysis which has been accomplished in their investigation denoted that the pressure ratio of the turbine has a significant effect on the exergy efficiency.Hydrogen has superior performance in comparison with all kinds of carbon-based fuels (hydrocarbon fuels) such as higher ignitability and greater flame stability for combustion. These intrinsic profits nowadays

have captured great attention in recent studies of H_2-fueled scramjet engines [18-20]. An optical diagnosis-based experimental study has been conducted by Wang et al [] to investigate the combustion modes of a cavity-based supersonic combustor of hydrogen-fueled jet at 6 much flight simulated conditions. Three combustion modes have been observed for cavity-assisted hydrogen combustion. The combined cavity shear-layer/recirculation stabilized combustion mode is introduced as the best performance combustion mode by this research results. Moreover, Sun et al [] in other research the sparks ignition process of hydrogen-fueled scramjet equipped with multi-cavities at 4 much flight condition has been studied by high-speed photography and Schlieren system with stagnation state of $T_0 = 846\,k$ and $P_0 = 0.7\,Mpa$. Their study results showed that the direct injection of H_2 to cavity can greatly improve the ignition process in combustion chamber of scramjet. H_2 production process is carried out by biomass conversion, steam methane reforming, or water splitting. Splitting water is a thermochemical process which is called electrolysis. There are three common forms of electrolyzing procedures, consist of oxidation of solid, alkaline, and proton exchange membrane (PEM) electrolysis. Hydrogen production via PEM electrolysis has numerous advantages particularly in renewable outline, including low environmental impact, being compact, containing no hazardous chemicals, and producing high pure hydrogen [21]. PEM is the most prevalent method of hydrogen production in energy systems with low-grade heat sources because of its high compatibility with these systems and is introduced as the commendable hydrogen production method for future utilities accordingly [22-24]. Leung et al. [25] performed thermodynamic and exergy studies of a PEM electrolyzer showing that hydrogen production and energy efficiency are significantly related to the PEM working temperature, electrode catalytic activity, and electrolyte wall thickness. Marangio et al. [26] presented a model for the theoretical study of the PEM cells in which a complicated pattern of Ohmic losses in electrodes and membrane. They have validated the presented model using available experimental data. In another work, carried out by Ahmadi et al. [27], a PEM electrolyzer which is actuated by solar energy, has been assimilated with an OHEC (ocean heat energy conversion) system to extract H_2. Energy and exergy analysis has been conducted in their proposed model and it is discovered that the extracted hydrogen is 1.2 kg/h with thermodynamic and exergy efficiencies of 3.6% and 23%, respectively. The importance of thermal management of the scramjet and its effects on the operation of this hypersonic vehicle has drawn the attention of many researchers it in recent years. The M-OCC is known as one of the most feasible systems for cooling scramjet engines [8]. On the other hand, some studies have tried to examine the exergy aspect of utilizing this kind of cooling system for co-production aims such as a limited exergy-based study conducted by Li and Wang [17]. Despite all efforts to study and outstrip these cooling systems or conducting thermodynamic analysis of these systems, the lack of an exclusive thermodynamic and exergy analysis of the M-OCC and investigating the effects of multi-expansion process is also indispensable. Moreover, no thoroughgoing investigation for producing electricity and hydrogen from waste heat of scramjet via PEM electrolyzer is presented up to yet. Based upon the above-discussed literature and reviewing similar researches in this field it is self-evident that extracting surplus amount of H_2 via electrolysis process and waste thermal heat of scramjet can be the best resolution to tackle high fuel consumption issue in the scramjet initiation. The aim of the present work is to advance a novel multi-stage OCC in order to produce electricity and hydrogen and cooling the scramjet engine as well. Additionally, a thoroughgoing study on multi-expansion effects is accomplished from the thermodynamic standpoint. In the proposed set-up, the PEM is driven by a portion of net output power in the cooling cycle, whilst the waste heat of scramjet is pondered as the heat source of the multi cooling cycle.

Nomenclature

c_p	specific heat capacity ($kJ.kg^{-1}.K^{-1}$)
D	membrane thickness (μm)

E	electrical energy (kJ)
ex	exergy rate per unit mass (kW/kg)
$\dot{E}x$	exergy rate (kW)
F	Faraday constant (C/mol)
G	Gibbs free energy (kJ.kmol^{-1})
Gen	generator
H	specific enthalpy per mole $(kJ.kmol^{-1})$
h	specific enthalpy per mass $(kJ.kg^{-1})$
J	current density (A.m^{-2})
J_a^{ref}	pre-exponential factor of anode (A.m^{-2})
J_c^{ref}	pre-exponential factor of cathode (A.m^{-2})
J_i^{ref}	pre-exponential factor (A.m^{-2})
LHV	lower heating value $(kJ.kg^{-1})$
$\dot{m}$	mass flow rate $(kg.s^{-1})$
$\dot{m}_0$	mass flow rate of fuel $(kg.s^{-1})$
$\dot{N}$	molar mass flow rate $(kmol.s^{-1})$
P	pressure (MPa)
Q	heat transfer energy (kJ)
$\dot{Q}$	heat transfer rate (kW)
R	PEM ohmic resistance (Ω)
S	specific entropy per mole $(kJ.kmol^{-1}.K^{-1})$
s	specific entropy per mass $(kJ.kg^{-1}.K^{-1})$
T	temperature (K)
V_0	reversible potential (V)
$V_{act,a}$	activation over-potential of anode (V)
$V_{act,c}$	activation over-potential of cathode (V)
V_0	reversible potential (V)
V	electrical potential (V)
w	specific power per mass unit (MW/kg)
$\dot{W}$	power rate (kW)
x	distance in membrane (m)
$Y_{D,i}$	exergy destruction ratio of the ith component (%)
y_i	concentration
Z_t	Purchased-equipment cost of turbine ($)

Acronyms

EES	Engineering Equation Solver
HE	heat exchanger
M-OCC	multi-stage OCC
OCC	open cooling cycle
PEM	proton exchange membrane
RCC	regenerative cooling cycle

Greek Symbols

η	efficiency (%)
δ	multiplication ratio
ϕ	reduction ratio
ρ	density (kg.m^{-3})
γ	heat capacity ratio
$\lambda(x)$	local ionic conductivity (Ω^{-1})
π	pressure ratio

Subscripts and superscripts

a	anode
act,a	activation of anode
act,c	activation of cathode
av	average
c	cathode
CH	chemical
CP	cooling passage
cr	critical
D	destruction
en	energy
ex	exergy
F	fuel
G	generator
i	ith component
int	intermediate
in	inlet
is	isentropic
j	jth stage
KN	kinetic
net	net value
out	outlet
P	product
p	pump
PH	physical
PT	potential
ref	reference
scr	scramjet
t	turbine

v	vapor
w	water
1,2,…	cycle locations
0	dead state

Greek Symbols

η	efficiency (%)
δ	multiplication ratio
ϕ	reduction ratio
ρ	density (kg.m^{-3})
γ	heat capacity ratio
$\lambda(x)$	local ionic conductivity (Ω^{-1})
π	pressure ratio

Subscripts and superscripts

a	anode
act,a	activation of anode
act,c	activation of cathode
av	average
c	cathode
CH	chemical
CP	cooling passage
cr	critical
D	destruction
en	energy
ex	exergy
F	fuel
G	generator
i	ith component
int	intermediate
in	inlet
is	isentropic
j	jth stage
KN	kinetic
net	net value
out	outlet
P	product
p	pump
PH	physical
PT	potential
ref	reference
scr	scramjet
t	turbine
v	vapor
w	water
1,2…	cycle locations
0	dead state

2. Cycle description

An illustrative configuration of the novel proposed set-up has been depicted in Fig 1. The system includes two main sub-cycles, power and PEM electrolyzer sub-cycles. The liquid hydrogen is pumped from scramjet fuel tank to the first cooling passage entry (state 2). Whilst H_2 constantly streams across the cooling passage, it rapidly turns to a supercritical gas by absorbing the heat of scramjet engine in which fuel works as a coolant. Then the superheated hydrogen enters the first turbine (state 3) and the hydrogen, under an isentropic condition, is expanded to produce electric power with the help of a coupled generator. Through this process H_2 is cooled down to T_4 (state 4). The cooled fuel coolant is heated up above the supercritical condition by flowing through the second passage (process 4 to 5) and again is cooled down by being expanded through turbine 2 (process 5 to 6). This process of heating the coolant to cool the combustion chamber, and cooling it down through the turbine to produce the electricity accomplishes two times more in the third and fourth cooling passages and two turbines (turbine 3 and turbine 4) that have been placed in outlet of this two cooling passages. Eventually, the last cooling process (process 10-11) occurs in the fifth cooling passage then the hydrogen leaves it (state11) and can be injected into the combustion chamber, as fuel. The PEM electrolyzer for hydrogen production requires electric power and heat. The electricity is supplied by M-OCC sub-system and heat comes from the waste heat of the scramjet combustion chamber as shown in Fig 1. Meanwhile, to bring the water up to the PEM temperature it first goes through the PEH heat exchanger (PEM-HE) at state 12, before entering to the electrolyzer (state 13). In the electrolysis process, H_2 began to leave the cathode side by a fair segment of the net electricity output and cools down to the ambient temperature (state 15). On the anode side O_2 separation from the water content occurs. The O_2 gas is cooled to ambient temperature and accumulated in the storage tank (state 14). The residual water content of the electrolyzer is recirculated by a water sub-supply pipeline for the next H_2 producing cycle. By carrying on the process sequentially, the H_2 will be produced and stored in a tank.

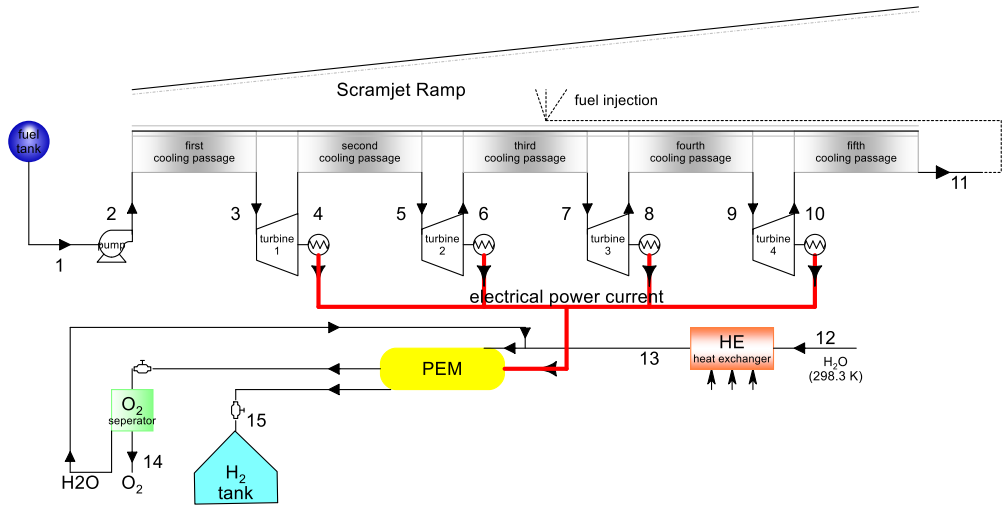

Fig. 1. Schematic diagram of the proposed novel scramjet multi-stage OCC coupled with a PEM electrolyzer

3. Presumptions and methodology

3.1. Presumptions

The following presumptions are made:

- Steady-state mathematical models
- The specific heat is considered to be constant
- The coolant is considered to be perfect gas , after the first cooling passage
- In cooling passages, pipelines and connections there is no pressure losses.
- In turbines, there is no heat transfer losses.
- The reference temperature is considered 298 K
- The reference pressure is considered 0.101 MPa
- Scramjet body temperature is considered to be constant and equal to scramjet body average temperature.
- At the entrance of the first cooling passage, Liquid H_2 has the pressure over critical pressure and its temperature is 25 K, well below the critical temperature (P_{cr}=1.3 MPa ,T_{cr} = 33 K [28]).
- Water enters the PEM electrolyzer at 298 K [29].
- The produced H_2 and O_2 are cooled to ambient temperature 298K [29].
- No energy losses in the electrolyzer process.

The presumptions aren't precise enough in order to get the actual design. Although, they are sufficient for the aim of this study.

3.2. Some basic definitions of performance criteria

The reduction of the fuel (as coolant) flow rate for cooling by improving the heat absorption per unit of fuel is the main purpose for OCC. Some parameters are needed to be defined for bringing into comparison the performance privileges of the multi-stage OCC and regenerative cooling cycles.

3.2.1 Multiplication ratio of the fuel heat absorption (δ)

If the Q_1 is considered to be the cooling of the first cooling passage and Q_2 cooling of the second cooling passage, multiplication ratio is defined as a parameter by which the cooling capacity improvement of each cooling passage stage in comparison with its previous stage can be assessed [8]. According to the above definition, the multiplication ratio of the second stage (Q_2) to its previous stages (Q_1) is expressed as:

$$\delta_1 = \frac{Q_2}{Q_1} \quad (1)$$

By the same definition, we can calculate: δ_1, δ_2, δ_3 for the third, fourth, and fifth cooling passages respectively. Thus we have:

$$\delta_2 = \frac{Q_3}{Q_1 + Q_2} \quad (2)$$

$$\delta_3 = \frac{Q_4}{Q_1 + Q_2 + Q_3} \quad (3)$$

$$\delta_4 = \frac{Q_5}{Q_1 + Q_2 + Q_3 + Q_4} \quad (4)$$

3.2.2 .Reduction ratio of the mass flow rate of fuel for cooling (ϕ)

The fuel heat absorption capacity augmentation is interpreted as a reduction in the mass flow rate of fuel (as coolant). In the other words, the straight impact of utilizing OCC in cooling system performance is to reduce the required fuel flow rate. In order to evaluate the capability of OCC in decreasing fuel flow rate, a reduction ratio of OCC should be defined. So the reduction ratio of the second cooling passage ($\emptyset_1$) can be written as [8]:

$$\phi_1 = \frac{Q_2}{Q_1 + Q2} \quad (5)$$

Similarly, $\emptyset_2$ to $\emptyset_4$ can be defined as reduction ratio of the third to the fifth cooling passages, respectively, as:

$$\phi_2 = \frac{Q_3}{Q_1 + Q_2 + Q_3} \quad (6)$$

$$\phi_3 = \frac{Q_4}{Q_1 + Q_2 + Q_3 + Q_4} \quad (7)$$

$$\phi_4 = \frac{Q_5}{Q_1 + Q_2 + Q_3 + Q_4 + Q_5} \quad (8)$$

3.3 PEM electrolyzer formulae

An illustrative configuration of the PEM electrolyzer sub-cycle is located in the bottom part of Fig.1, as it can be observed. The PEM electrolyzer produces hydrogen by water splitting process, an electrochemical reaction in which the electricity and heat are utilized as energy suppliers. Hence, an electrochemical-based modeling is required to appraise the PEM from the thermodynamic and Exergetic prospects.

The summation of needed thermal energy (TΔS) and ΔG (Gibb's free energy) of reaction attains the overall energy requirement [28], as below:

$$\Delta H = \Delta G + T\Delta S \quad (9)$$

The rate of H_2 molar mass flow is accessed by [29]:

$$\dot{N}_{H_{2out}} = \frac{J}{2F} = \dot{N}_{H_2O,reacted} \quad (10)$$

F is a constant (Faraday constant) and J is called the current density. The electrical power entrance rate to the electrolyzer is derived as:

$$E_{electric} = JV \quad (11)$$

Also, V is given as:

$$V = V_0 + V_{act,a} + V_{act,c} + V_{ohm} \quad (12)$$

where V_0 is the reversible potential and V_0 is extracted by the Nernst equation as below [29]:

$$V_0 = 1.229 - 8.5\times10^{-4}\left(T_{PEM} - 298\right) \quad (13)$$

Also, $V_{act,c}$, $V_{act,a}$ and V_{ohm} are described as the cathode activation overpotential, the anode activation overpotential, and the Ohmic overpotential of the electrolyte, correspondingly. The ionic conductivity at each region of the PEM membrane $\lambda(x)$ is addressed as [30,31]:

$$\sigma_{PEM}[\lambda(x)] = [0.5139\lambda(x) - 0.326]\exp\left[1268\left(\frac{1}{303} - \frac{1}{T}\right)\right] \quad (14)$$

x is the calculated distance from the cathode side surface. The quantity of $\lambda(x)$ can be acquired by:

$$\lambda(x) = \frac{\lambda_a - \lambda_c}{D}x + \lambda_c \quad (15)$$

λ_a and λ_c are used to represent the water quantity of anode and cathode membranes at their surfaces correspondingly and D denotes the thickness of the used membrane. The PEM Ohmic resistance is drafted as [29]:

$$R_{PEM} = \int_0^D \frac{dx}{\sigma_{PEM}[\lambda(x)]} \quad (16)$$

The ohmic overpotential equation is expressed as below by the use of Ohm's potential law [30]:

$$V_{ohm,PEM} = JR_{PEM} \quad (17)$$

Accordingly, the activation overpotential ($V_{act,i}$) is ascertained as [31]:

$$V_{act,i} = \frac{RT}{F}\sinh^{-1}\left(\frac{J}{2J_{a,i}}\right), i = a, c \quad (18)$$

J_0 is the exchange current density for electrolyzer which is addressed as [25]:

$$J_{0,i} = J_i^{ref} \exp\left(-\frac{E_{act,i}}{RT}\right), i = a, c \quad (19)$$

$E_{act,i}$ is the activation electricity of PEM (for both anode and cathode sides) and J_i^{ref} is called the pre-exponential factor of function. Many other studies have been conducted the PEM modeling more specifically [32, 33].

3.4 Thermodynamic analysis

In this section, energetic and exergetic examination and some other mathematical determinations of the advanced system, such as multi-expansion evaluation, are explained in detail. Every single constituent of the system are regarded as control volume. The thermodynamic conservation balance beside the exergy equations is exerted to each component, individually.

The general steady-state forms of mass and energy balance equations for any control volume can be applied as [28]: [28]:

$$\sum \dot{m}_{in} = \sum \dot{m}_{out} \quad (20)$$

$$\dot{Q} - \dot{W} = \sum \dot{m}_{out} h_{out} - \sum \dot{m}_{in} h_{in} \quad (21)$$

The energy efficiency of the recommended cycle is ascertained as the sum of the produced hydrogen energy and net electricity output of the cycle divided by energy intake (absorbed heat from cooling passages and PEM-HE) which is addressed as:

$$\eta_{en} = \frac{LHV_{H_2}.\dot{m}_{15} + (1-\eta_G).\dot{W}_{net}}{\dot{Q}_{total}} \quad (22)$$

LHV_{H_2} is Latent Heat Value of H_2 that should be obtained from thermodynamic references which is 120.211 (kJ/kg) [34]. And $\dot{Q}_{total}$ is the total cooling of the scramjet engine which is used as the heat source of the system (Table 1). Considering a turbine that goes on an isentropic process between state b and c, as shown in Fig. 2.

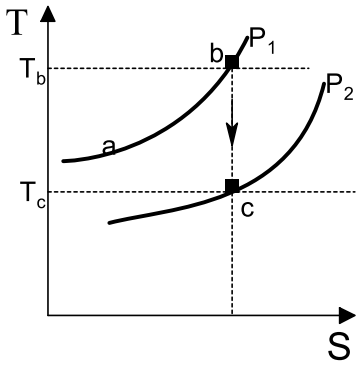

Fig. 2. Schematic T-S diagram of an isentropic expansion process in a turbine

Table 1. Energy balance equations for each component of the simulated set-up.

Parameters	Equation
Heat load of cooling passage 1	$\dot{Q}_1 = \dot{m}_1 c_p (T_3 - T_2)$
Heat load of cooling passage 2	$\dot{Q}_2 = \dot{m}_2 c_p (T_5 - T_4)$
Heat load of cooling passage 3	$\dot{Q}_3 = \dot{m}_3 c_p (T_7 - T_6)$
Heat load of cooling passage 4	$\dot{Q}_4 = \dot{m}_4 c_p (T_9 - T_8)$
Heat load of cooling passage 5	$\dot{Q}_5 = \dot{m}_5 c_p (T_{11} - 10)$
Specific work of turbine 1	$w_{t1} = \eta_t c_p T_3 \left[1 - {\pi_1}^{(1-\gamma)/\gamma}\right]$
Specific work of turbine 2	$w_{t2} = \eta_t c_p T_5 \left[1 - {\pi_2}^{(1-\gamma)/\gamma}\right]$
Specific work of turbine 3	$w_{t3} = \eta_t c_p T_7 \left[1 - {\pi_3}^{(1-\gamma)/\gamma}\right]$
Specific work of turbine 4	$w_{t4} = \eta_t c_p T_9 \left[1 - {\pi_4}^{(1-\gamma)/\gamma}\right]$
Specific work of pump	$w_p = \frac{P_2 - P_1}{\eta_p \rho_1}$
Specific net power	$w_{net} = w_{t1} + w_{t2} + w_{t3} + w_{t4} - w_p$
Net electricity	$\dot{W}_{net} = \dot{m}_0 w_{net}$
Heat load of heat exchanger	$\dot{Q}_{HE} = \dot{m}_w (h_{13} - h_{12})$
Total cooling	$\dot{Q}_{total} = \dot{Q}_1 + \dot{Q}_2 + \dot{Q}_3 + \dot{Q}_4 + \dot{Q}_5 + \dot{Q}_{HE}$

And assuming that the turbine works without any power losses because of mechanical friction, from thermodynamic relations, the outlet temperature of the turbine can be achieved as [28]:

$$T_c = T_b \left\{1 - \eta_t \left[1 - \pi^{(1-\gamma)/\gamma}\right]\right\} \tag{23}$$

By the use of Eq. (23), the specific power output of the turbine can be derived as:

$$w_t = \eta_t C_p T_b \left[1 - \pi^{(1-\gamma)/\gamma}\right] \tag{24}$$

π is the pressure ratio that is the division of inlet and outlet pressures of the turbine:

$$\pi = \frac{p_b}{p_c} \tag{25}$$

By using Eq. (4) in the multiplication and reduction ratios the following relations can be rewritten as:

$$\delta_i = \frac{\eta_t T_b \left[1 - \pi^{(1-\gamma)/\gamma}\right]}{T_c - T_b} \tag{26}$$

$$\phi_i = \frac{\eta_t T_c \left[1 - \pi^{(1-\gamma)/\gamma}\right]}{T_c - T_b + \eta_t T_c \left[1 - \pi^{(1-\gamma)/\gamma}\right]} \tag{27}$$

Table 1 comprises some of the significant thermodynamic equations computed by energetic and mass balances.

The rate of total exergy of a flow ($\dot{E}x_{total}$) consist of four main components: physical exergy rate ($\dot{E}x_{PH}$), kinetic exergy rate ($\dot{E}x_{KN}$), potential exergy rate ($\dot{E}x_{PT}$), and chemical exergy rate ($\dot{E}x_{CH}$) [35]:

$$\dot{E}x_{total} = \dot{E}x_{PH} + \dot{E}x_{KN} + \dot{E}x_{PT} + \dot{E}x_{CH} \tag{28}$$

Among those four components, kinetic and potential exergies are usually postulated trivial. The rate of physical exergy of a closed system is acquired as below:

$$\dot{E}x_{Ph} = \dot{m}(h - h_0 - T_0(s - s_0)) \tag{29}$$

Also for the chemical exergy rate we have:

$$\dot{E}x_{ch} = \dot{m}\left[\sum_{i=1}^{n} x_i ex_{ch,i} + RT_0 \sum_{i=1}^{n} x_i \ln x_i\right] \tag{30}$$

In which, x_i is used for the molar concentration and $ex_{ch,i}$ shows the specific chemical exergy of the material that is reachable in all thermodynamic references.

The balanced equation of the exergy rates for an element such as i can be stated as:

$$\dot{E}x_F^i = \dot{E}x_P^i + \dot{E}x_D^i \tag{31}$$

$\dot{E}x_D^i$ is the rate of exergy destruction as well, $\dot{E}x_F^i$ and $\dot{E}x_P^i$ are fuel and product exergy rates of component i respectively.

In the same way, the balance equation for the overall system can be considered as:

$$\dot{E}x_F^{total} = \dot{E}x_P^{total} + \dot{E}x_D^{total} \tag{32}$$

exergetic efficiency of element i (η_{ex}^i) is derived as:

$$\eta_{ex}^i = \dot{E}x_P^i / \dot{E}x_F^i \tag{33}$$

To compare the exergetic destruction of each component of the system with other components the destruction percentage, also is called effective defect, is used as follow:

$$y_{D,i} = \dot{E}x_{D,i} / \dot{E}x_{D,total} \tag{34}$$

The total exergetic efficiency of the system can be considered the same as Eq.(34):

$$\eta_{ex}^{total} = \dot{E}x_P^{total} / \dot{E}x_F^{total} \tag{35}$$

Table 2 provides some of the important exergy based balance equations of the introduced set-up that are needed to assess the exergy of the components, suited to the exegy balance relations.

4. Results and discussion

An appropriate EES code based on section 3.1 mentioned assumptions has been developed to analyze the system from energetic and exergetic prospects. To run the simulation code and obtain the outputs some input data are needed. Table 3 listed the reliable input parameters to simulate the cycle. Additionally, Table 4 listed some other input data for the simulation of the PEM electrolyzer. By running developed code, some key parameters of the flow have been gained (Table 5) as an outcome of this simulation. These thermodynamic parameters consist of temperature, pressure, mass flow, enthalpy, entropy, and exergy rates at each state.

Table 2: Exergy equations of main components of the simulated system

Component	Exergy of fuel	Exergy of product	Exergy of destruction	Exergetic efficiency	Exergy destruction ratio
Cooling passage 1	$\dot{E}x_{F,CP1} = \dot{Q}_1\left(1-\frac{T_0}{T_{ref-scr}}\right)$	$\dot{E}x_{P,CP1} = \dot{E}x_3 - \dot{E}x_2$	$\dot{E}x_{D,CP1} = \dot{E}x_{F,CP1} - \dot{E}x_{P,CP1}$	$\eta_{ex,CP1} = \frac{\dot{E}x_{P,CP1}}{\dot{E}x_{F,CP1}}$	$Y_{D,CP1} = \frac{\dot{E}x_{D,CP1}}{\dot{E}x_{D,total}}$
Cooling passage 2	$\dot{E}x_{F,CP2} = \dot{Q}_2\left(1-\frac{T_0}{T_{ref-scr}}\right)$	$\dot{E}x_{P,CP2} = \dot{E}x_5 - \dot{E}x_4$	$\dot{E}x_{D,CP2} = \dot{E}x_{F,CP2} - \dot{E}x_{P,CP2}$	$\eta_{ex,CP2} = \frac{\dot{E}x_{P,CP2}}{\dot{E}x_{F,CP2}}$	$Y_{DCP2} = \frac{\dot{E}x_{D,CP2}}{\dot{E}x_{D,total}}$
Cooling passage 3	$\dot{E}x_{F,CP3} = \dot{Q}_3\left(1-\frac{T_0}{T_{ref-scr}}\right)$	$\dot{E}x_{P,CP3} = \dot{E}x_7 - \dot{E}x_6$	$\dot{E}x_{D,CP3} = \dot{E}x_{F,CP3} - \dot{E}x_{P,CP3}$	$\eta_{ex,CP3} = \frac{\dot{E}x_{P,CP3}}{\dot{E}x_{F,CP3}}$	$Y_{D,CP3} = \frac{\dot{E}x_{D,CP3}}{\dot{E}x_{D,total}}$
Cooling passage 4	$\dot{E}x_{F,CP4} = \dot{Q}_4\left(1-\frac{T_0}{T_{ref-scr}}\right)$	$\dot{E}x_{P,CP4} = \dot{E}x_9 - \dot{E}x_8$	$\dot{E}x_{D,CP4} = \dot{E}x_{F,CP4} - \dot{E}x_{P,CP4}$	$\eta_{ex,CP4} = \frac{\dot{E}x_{P,CP4}}{\dot{E}x_{F,CP4}}$	$Y_{D,CP4} = \frac{\dot{E}x_{D,CP4}}{\dot{E}x_{D,total}}$
Cooling passage 5	$\dot{E}x_{F,CP5} = \dot{Q}_5\left(1-\frac{T_0}{T_{ref-scr}}\right)$	$\dot{E}x_{P,CP5} = \dot{E}x_{11} - \dot{E}x_{10}$	$\dot{E}x_{D,CP5} = \dot{E}x_{F,CP5} - \dot{E}x_{P,CP5}$	$\eta_{ex,CP5} = \frac{\dot{E}x_{P,CP5}}{\dot{E}x_{F,CP5}}$	$Y_{D,CP5} = \frac{\dot{E}x_{D,CP5}}{\dot{E}x_{D,total}}$
Turbine 1	$\dot{E}x_{F,t1} = \dot{E}x_3 - \dot{E}x_4$	$\dot{E}x_{P,t1} = \dot{m}_1 w_{t1}$	$\dot{E}x_{D,t1} = \dot{E}x_{F,t1} - \dot{E}x_{P,t1}$	$\eta_{ex,t1} = \frac{\dot{E}x_{P,t1}}{\dot{E}x_{F,t1}}$	$Y_{D,t1} = \frac{\dot{E}x_{D,t1}}{\dot{E}x_{D,total}}$
Turbine 2	$\dot{E}x_{F,t2} = \dot{E}x_5 - \dot{E}x_6$	$\dot{E}x_{P,t2} = \dot{m}_2 w_{t2}$	$\dot{E}x_{D,t2} = \dot{E}x_{F,t2} - \dot{E}x_{P,t2}$	$\eta_{ex,t2} = \frac{\dot{E}x_{P,t2}}{\dot{E}x_{F,t2}}$	$Y_{D,t2} = \frac{\dot{E}x_{D,t2}}{\dot{E}x_{D,total}}$
Turbine 3	$\dot{E}x_{F,t3} = \dot{E}x_7 - \dot{E}x_8$	$\dot{E}x_{P,t3} = \dot{m}_3 w_{t3}$	$\dot{E}x_{D,t3} = \dot{E}x_{F,t3} - \dot{E}x_{P,t3}$	$\eta_{ex,t3} = \frac{\dot{E}x_{P,t3}}{\dot{E}x_{F,t3}}$	$Y_{D,t3} = \frac{\dot{E}x_{D,t3}}{\dot{E}x_{D,total}}$
Turbine 4	$\dot{E}x_{F,t4} = \dot{E}x_9 - \dot{E}x_{10}$	$\dot{E}x_{P,t4} = \dot{m}_4 w_{t4}$	$\dot{E}x_{D,t4} = \dot{E}x_{F,t4} - \dot{E}x_{P,t4}$	$\eta_{ex,t4} = \frac{\dot{E}x_{P,t4}}{\dot{E}x_{F,t4}}$	$Y_{D,t4} = \frac{\dot{E}x_{D,t4}}{\dot{E}x_{D,total}}$
Pump	$\dot{E}x_{F,p} = \dot{m}_1 w_p$	$\dot{E}x_{P,p} = \dot{E}x_2 - \dot{E}x_1$	$\dot{E}x_{D,p} = \dot{E}x_{F,p} - \dot{E}x_{P,p}$	$\eta_{ex,p} = \frac{\dot{E}x_{P,p}}{\dot{E}x_{F,p}}$	$Y_{D,p} = \frac{\dot{E}x_{D,p}}{\dot{E}x_{D,total}}$
PEM	$\dot{E}x_{F,PEM} = (1-\eta_G)\dot{W}_{net}$	$\dot{E}x_{P,PEM} = \dot{E}x_{14} + \dot{E}x_{15}$	$\dot{E}x_{D,PEM} = \dot{E}x_{F,PEM} - \dot{E}x_{P,PEM}$	$\eta_{ex,PEM} = \frac{\dot{E}x_{P,PEM}}{\dot{E}x_{F,PEM}}$	$Y_{D,PEM} = \frac{\dot{E}x_{D,PEM}}{\dot{E}x_{D,total}}$
Heat exchanger	$\dot{E}x_{F,HE} = \dot{Q}_{HE}\left(1-\frac{T_0}{T_{ref-scr}}\right)$	$\dot{E}x_{P,HE} = \dot{E}x_{13} - \dot{E}x_{12}$	$\dot{E}x_{D,HE} = \dot{E}x_{F,HE} - \dot{E}x_{P,HE}$	$\eta_{ex,HE} = \frac{\dot{E}x_{P,HE}}{\dot{E}x_{F,HE}}$	$Y_{D,HE} = \frac{\dot{E}x_{D,HE}}{\dot{E}x_{D,total}}$

Table 3: Some of the required input data for simulation of the system.

Parameter	**value**
Backpressure of pump, $P_2(MPa)$	22
The average temperature of scramjet body, $T_{av}(K)$	1000
Scramjet combustion chamber pressure, $P_{11}(MPa)$	1
Fuel tank temperature, $T_1(K)$	25
Fuel tank pressure, $P_1(MPa)$	0.24
Mass flow rate of fuel, $\dot{m}_0(kg/s)$	0.4
Mass flow rate of PEM entrance water, $\dot{m}_{12}(kg/s)$	0.0311
PEM entrance water temperature, $T_{12}(K)$	298
PEM temperature, $T_{PEM}(K)$	353
Turbine efficiency, η_t	0.8
Pump efficiency, η_p	0.7
Generator power efficiency, η_G	0.65

Table 4: Input parameters are used to model the PEM [35]

Parameter	**value**
$P_{O_2}(MPa)$	0.1
$P_{H_2}(MPa)$	0.1
$T_{PEM}(K)$	353
$E_{act,a}(kJ/mol)$	76
$E_{act,c}(kJ/mol)$	18
$\lambda_a\ (\Omega^{-1})$	14
$\lambda_c\ (\Omega^{-1})$	10
$D(\mu m)$	100
$J_c^{ref}(A/m^2)$	1.7×10^5
$J_a^{ref}(A/m^2)$	4.6×10^3
$F(C/mol)$	96486

Table 5: Thermodynamic properties in each state of the simulated system.

State	**Fluid**	$\boldsymbol{T(K)}$	$\boldsymbol{P(MPa)}$	$\boldsymbol{\dot{m}(kg/s)}$	$\boldsymbol{h(kJ/kg)}$	$\boldsymbol{s(kJ/kg.K)}$	$\dot{E}x\ (kW)$
1	Hydrogen	25	0.24	0.4	479.4	20.25	2510
2	Hydrogen	54.9	22	0.4	579.8	20.25	2551
3	Hydrogen	1000	22	0.4	14387	48.83	4758
4	Hydrogen	714.4	4.69	0.4	10010	50.22	2846
5	Hydrogen	1000	4.69	0.4	14235	55.19	3959
6	Hydrogen	841.5	2.166	0.4	11856	55.81	2936
7	Hydrogen	1000	2.166	0.4	14213	58.38	3581
8	Hydrogen	916.4	1.472	0.4	12959	58.67	3045
9	Hydrogen	1000	1.471	0.4	14207	59.97	3393
10	Hydrogen	916.4	1	0.4	12954	60.26	2859
11	Hydrogen	1000	1	0.4	14202	61.57	3207
12	Water	290	0.101	0.0321	70.75	0.251	77.51
13	Water	353	0.101	0.0321	334.3	1.073	78.31
14	Oxygen	353	0.101	0.0929	50.36	0.156	12.04
15	Hydrogen	353	0.101	0.01171	4720	55.81	2.379

4.1 Model validation

To evaluate the rectitude of our simulation modeling each of the sub-systems has been validated with the literature [8, 27] and the results of the current work indicated great conformity with their reported results. The validation result is shown in Fig.3 respectively.

4.2 Thermodynamic analysis results

The thermodynamic modeling results have been presented in this section. The developed code was conducted by input data to calculate the required parameters and the energy outcomes of the introduced cycle, listed in Table 7. For a mass flow rate of 0.4 (kg/s), the produced net electricity of cycle is 3386 (kW) and hydrogen production is 42.14 (kg/h) when the 65 percent of produced electricity be reachable for PEM as the power input. Thus the overall energy efficiency of the proposed system, in which the electricity and hydrogen are as products, is about 13.07%. The energy efficiency of the system is supposed to be good by consideration of using a low-grade heat source (waste heat), as we know low-grade heat sources have low efficiencies. The hydrogen production quantity is noteworthy in comparison with other similar systems' production. Such high hydrogen production systems would have numerous usages in the aerospace industry. The cooling capacity of the proposed system is 9.16 MW . It can be figured out that the proposed cooling cycle is suitable for a scramjet with an average wall temperature of 1000 k at 8 much flight conditions in which the heat flux per unit area of the wall is about 1.5 MW per unit of wall area.

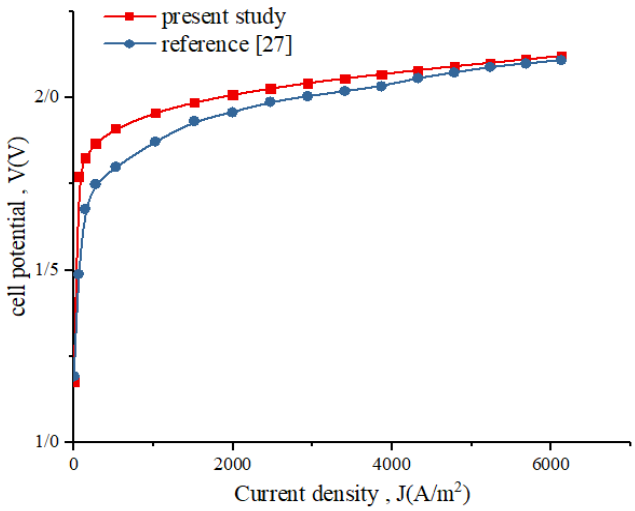

Fig. 4. The PEM electrolyzer model validation of the present study with reference [27]

Table 6: Energy evaluation results obtained from simulation

parameter	**Value**
First cooling passage heat load, $\dot{Q}_1(kW)$	5523
Second cooling passage heat load, $\dot{Q}_2(kW)$	1690
Third cooling passage heat load, $\dot{Q}_3(kW)$	942.5
Fourth cooling passage heat load, $\dot{Q}_4(kW)$	499.2
Fifth cooling passage heat load, $\dot{Q}_5(kW)$	499.2
Pump power, $w_p(MJ/kg)$	0.4353
Turbine 1 power, $w_{t1}(MJ/kg)$	4.158

Turbine 2 power, $w_{t2}(MJ/kg)$	2.308
Turbine 3 power, $w_{t3}(MJ/kg)$	1.217
Turbine 4 power, $w_{t4}(MJ/kg)$	1.217
Net electricity output, $\dot{W}_{net}(kW)$	3386
PEM power entrance, $\dot{W}_G(kW)$	2201
Hydrogen production, $\dot{m}_{H_2}(kg/h)$	42.14
PEM heat exchanger load, $\dot{Q}_{HE}(kW)$	8.461
Total cooling, $\dot{Q}_{total}(kW)$	9162
Energy efficiency overall system, $\eta_{en}(\%)$	12.95
Multiplication ratio of second cooling passage, δ_1	0.3022
Multiplication ratio of third cooling passage, δ_2	0.1086
Multiplication ratio of fourth cooling passage, δ_3	0.0398
Multiplication ratio of fifth cooling passage, δ_4	0.03978
Reduction ratio of second cooling passage, ϕ_1	0.2321
Reduction ratio of third cooling passage, ϕ_2	0.07544
Reduction ratio of fourth cooling passage, ϕ_3	0.029968
Reduction ratio of fifth cooling passage, ϕ_4	0.02967

The results of the exergy study have been obtained as presented in Table 8. The overall system exergy efficiency is 22.16 %. The PEM electolyzer with a relative exergy destruction ratio of more than 47 percentage (Fig. 4) has the least exergy efficiency among the system components. This amount of high exergy destruction is engendered by the irreversibility of the chemical reaction of the water electrolyzing process [36]. After the PEM electrolyzer, the first cooling passage has the highest exergy destruction with more than 37 percentage of exergy destruction ratio of overall destruction and this is because of the very high-temperature difference that heat transferring is occurring in it. The exergy destruction is in direct proportion to temperature difference [29]. These two high destruction rate components of the system are clearly shown in Fig. 5.

Table 7: Exergy study results of proposed cycle

Component	$\dot{Ex}_F(kW)$	$\dot{Ex}_P(kW)$	$\dot{Ex}_D(kW)$	$\eta_{ex}(\%)$	$Y_D(\%)$
First cooling passage	3921	2207	1714	56.28	37.23
Second cooling passage	1200	1113	86.63	92.78	1.882
Third cooling passage	669.4	645.2	24.2	96.38	0.5256
Fourth cooling passage	354.4	348	6.403	98.19	0.1391
Fifth cooling passage	354.4	348	6.403	98.19	0.131
Pump	174.1	40.14	134	23.05	2.91
Turbine 1	1912	1663	284.6	87	5.399
Turbine 2	1024	923.1	100.5	90.18	2.182
Turbine 3	535.3	487	48.28	90.98	1.049
Turbine 4	534.5	487	47.5	91.11	1.032
PEM	2201	14.42	2187	0.6551	47.49
PEM heat exchanger	1.883	0.8046	1.078	42.74	0.02341
Overall system	6501	1440	5061	22.16	-

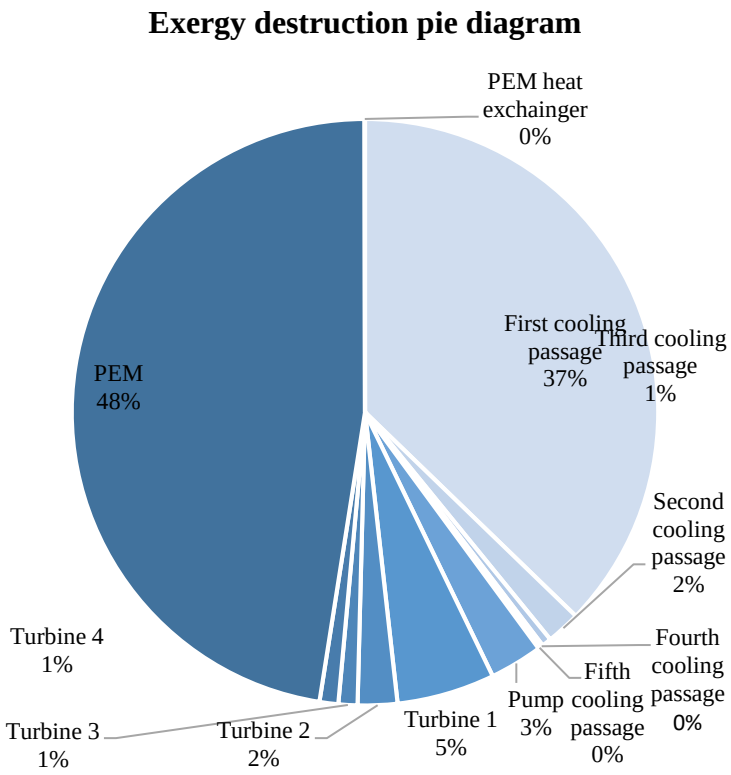

Fig. 5. Exergy destruction distribution of system components

4.4 Parametric study

In the present part, the impacts of some significant parameters on the important outputs of our system have been investigated. The mass flow rate of fuel, the backpressure of the pump, scramjet body temperature, and generator power efficiency are chosen to be studied because these parameters had the most significant effects on the system.

4.4.1 The impact of mass flow rate of fuel on the system

In Fig. 8 has been shown the effects of the mass flow rate of the scramjet fuel on the net electricity output, total cooling, hydrogen production as well as energy and exergy efficiencies. All three main purposes of advanced set-up including, scramjet cooling, electricity, and hydrogen production increase when the mass flow rate of fuel is increased (Fig. 8.a). As we know, the electricity production and heat absorption of cooling passages have a direct proportion to the mass flow rate of fuel. On the other hand, the flow energy difference (flow enthalpy difference) of states has remained constant thus the mass flow rate augmentation leads to electricity production and cooling increase. The electricity production increment in power sub-cycle, in which a segment of produced electricity drives the PEM electrolyzer sub-cycle, causes a rise in the current density of the electrolyzer. Therefore the H_2 production increases regarding Eq. 10. The energy and exergy efficiencies of the whole cycle are approximately constant with any variation in the mass flow rate. This can be reasonable by considering the matter that mass flow rate augmentation results in higher electricity and hydrogen production. But, as it can be observed, the absorbed heat of cooling passages which is the heat sources of the proposed system also rises, as the same scale of productions. So the energy and exergy efficiencies remain about constant, as we can see in Fig. 8.b.

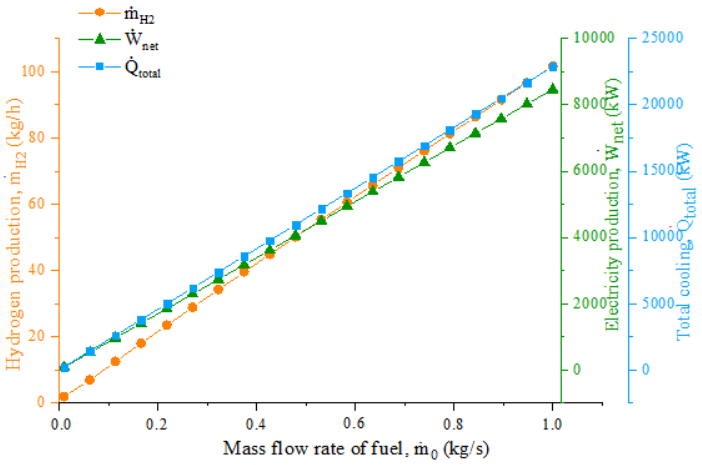

8(a)

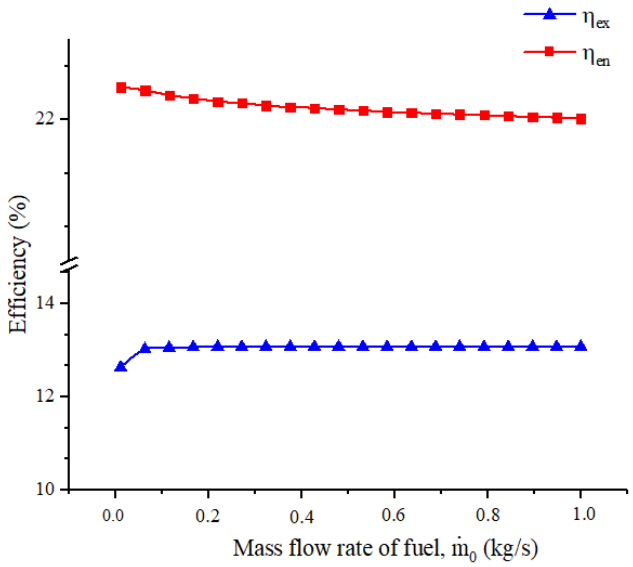

8(b)

Fig. 8. The impact of the mass flow rate of fuel on: (a) net electricity production, hydrogen production and total cooling, (b) exergy and energy efficiencies

4.4.2 The impact of pump back pressure on the system

Backpressure of the pump effect on the main output parameters of the system is shown in Fig. 9. The electricity output and the amount of scramjet cooling go up by pump back pressure increment Fig. 9.a. The backpressure of pump accretion means expansion ratio increase, higher pressure drop, and higher temperature drop through the expansion process. The power relation of the turbine tells us that the power production has direct relevance with expansion ratio. On the other hand, higher temperature difference in heat transfer is equal to higher heat transferring (based upon heat transfer principles). Accordingly, backpressure increase in constant mass flow rate causes electricity production and cooling increase. As mentioned above, the electricity production increment leads to hydrogen production augmentation. Also the total cooling (that is heat source of the cycle) and two production parameters of the system both increase but the augmentation rate of production is sensibly more and results in energy and exergy efficiencies improvements, Fig. 9.b represents that.

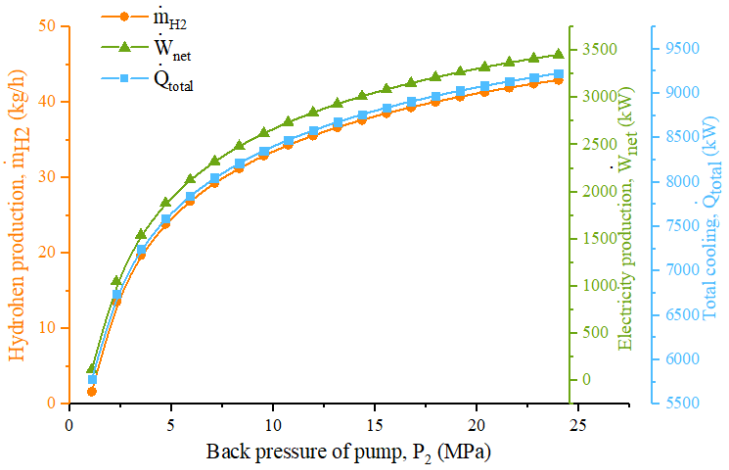

9(a)

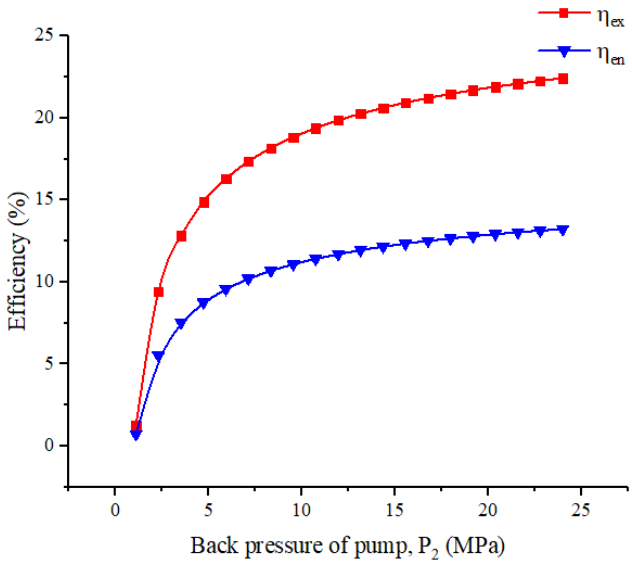

9(b)

Fig. 9. The pump back pressure effect on: (a) the hydrogen and net electricity production and (b) the energy and exergy efficiencies

4.4.3.The impact of scramjet body temperature on the cycle

Increasing the scramjet body temperature shows a growing behavior on the three main outputs of the system including, the cooling load, electricity, and hydrogen production, as presented in Fig. 10.a. higher scramjet body temperature means higher enthalpy of fuel coolant at cooling passages output (turbines input) and we know that electricity production and cooling process (heat transfer) is in direct proportional with enthalpy difference thus both will show increasing behavior with body temperature increasing at which the mass flow rate of flow is constant. On the other hand, increasing electricity production cause hydrogen production increase which is explained in the above sections that why it happens. As a result of scramjet body temperature increasing, both main efficiencies (energy and exergy efficiencies) of the system do not change sensibly. Because the cooling heat absorption increment rate, which is the main heat source of the cycle, and the resultant products increment rate are approximately on the same scale, Fig. 10.b.

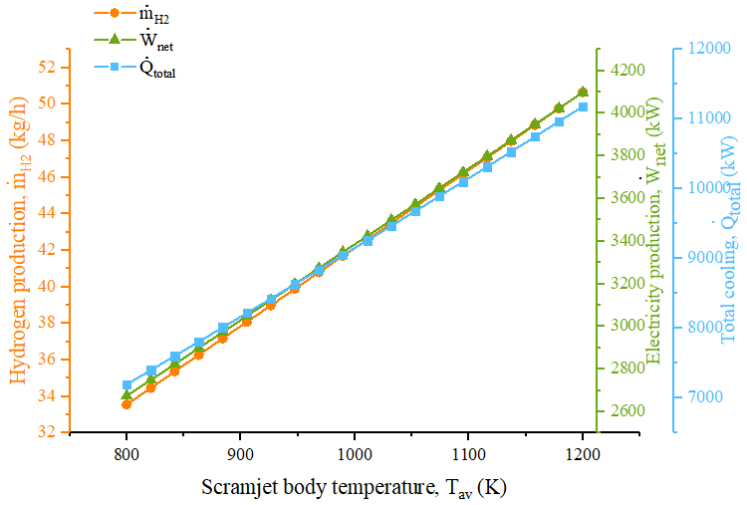

10(a)

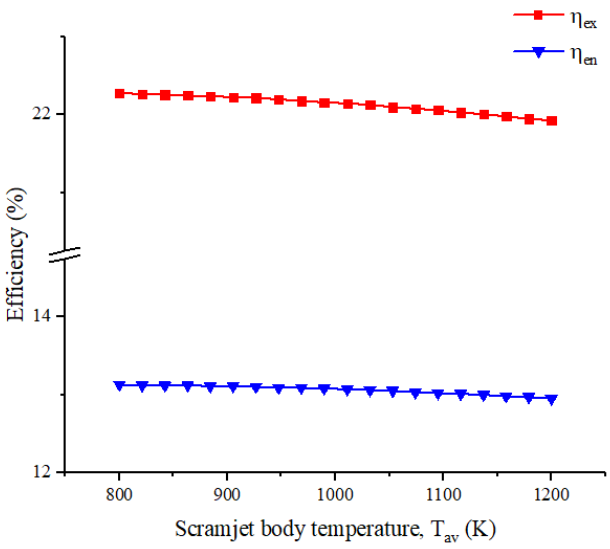

10(b)

Fig. 10. The scramjet body temperature variation effects on: (a) the hydrogen and electricity production as well as cooling load, (b) the energy and exergy efficiencies

4.4.4. The effect of generator power efficiency (η_{GP}) on the hydrogen production

The portion of extracted electricity of the system that is available for PEM electrolyzer as power entrance is denoted by generator power efficiency (η_{GP}). The effect of η_{GP} hydrogen production is depicted in Fig. 10. As it can be observed the hydrogen production rate augments reasonably. As a matter of fact, the higher η_{GP}means higher PEM electrolyzer entrance power which leads to hydrogen production increase accordingly.

5. Conclusions

In this study, a M-OCC has been introduced to produce electricity and hydrogen (by employing PEM electrolyzer) alongside the main purpose of scramjet body cooling. The power production sub-section is driven by the waste heat of cooling passages of scramjet and a distinct portion of net electricity output is employed for driving the PEM electrolyzer. Energetic and exergetic investigation of the advanced set-up and multi-expansion effects study has been accomplished to determine the operation of the system. Moreover, an exhaustive parametric

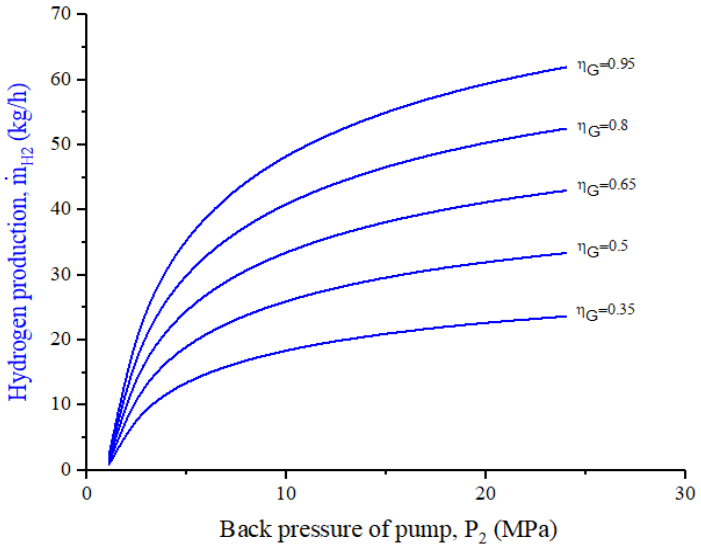

Fig. 11. The impact of generator power efficiency on the H_2 production rate in back pressure of pump variation range

investigation on some important thermodynamic parameters of the proposed cycle has been accomplished to have a better understanding of its operation. Some remarkable results can be outlined as follow:

- The net electricity production and the cooling load of scramjet rates are 3386 (kW) and 9162 (kW) correspondingly. Whilst, the H_2 production rate is obtained 42.14 (kg/h).
- The overall energy and exergy efficiencies of the developed system are gained 12.95 % and 22.16 %, sequentially.
- The exergy investigation results demonstrated that PEM electrolyzer has the maximum exergy destruction rate of 47.49 % and after PEM the first cooling passage has the second rank of the maximum exergy destruction rate by about 38 %. These two great destructions stem from two main resources of the irreversibility of systems, chemical reaction, and high-temperature difference.
- The electricity and hydrogen production and total cooling capacity are increased when the mass flow rate of fuel, back pressure of pump and scramjet body temperature rise.
- The energy and exergy performances of the cycle remain approximately constant with increasing of the mass flow rate of fuel whereas improved with pump back pressure increment. And the scramjet body temperature variation does not have any tangible effects on the whole energy and exergy efficiencies of the cycle.

References

[1] Heiser WH, Pratt DT. Hypersonic airbreathing propulsion. AIAA education series, Washington, DC: AIAA; 1994. P. 1-26.

[2] Edward T. Curran, Scramjet engines: the first forty years, J. propul. Power 17(6) (2001) 1138-1148.

[3] Hossain, Mohammad Arif & Rahman, Taibur & Hossain, Sarzina. (2014). Investigation and Improvement of Thermal Efficiency of Hypersonic Scramjet. ASME International Mechanical Engineering Congress and Exposition, Proceedings (IMECE). 1. 10.1115/IMECE2014-37385.

[4] Daniau, E. and Bouchez, M. Fuel reforming for scramjet thermal management and combustion optimization. AIAA paper 2005-340, 2005.

[5] Kanda, T., Masuya, G., and Wakamatsu, Y. Propellant feed system of a regeneratively cooled scramjet. J. Propuls. Power, 1991, 7(2), 299–301.

[6] Youn, B. and Millst, A. F. Cooling panel optimization for the active cooling system of a hypersonic aircraft. J. Thermophys. Heat Transf., 1995, 9(1), 136–143.

[7] Felix, F. C.,William, F. T.,Nancy,R. S., and Richard, B. N. An innovative thermal management system for a mach 4 to mach 8 hypersonic scramjet engine. AIAA paper 1998-3734, 1998.

[8] J. Qin, W. Bao, W. Zhou, D. Zhang, performance cycle analysis of an open cooling cycle for a scramjet. DOI: 10.1243/09544100JAERO552.

[9] W. Bao, J. Qin, W. Zhou, D. Zhang, D. Yu, Power generation and heat sink improvement characteristics of recooling cycle for thermal cracked hydrocarbon fueled scramjet, Sci. China, Technol. Sci. 54 (2011) 955–963.

[10] Cho H, Smith AD, Mago P. Combined cooling, heating and power: a review of performance improvement and optimization. Appl Energy 2014;136:168–85.

[11] Jiang, L., Wang, L.W., Liu, C.Z., Wang, R.Z., 2016. Experimental study on a resorption system for power and refrigeration cogeneration. Energy 97, 182–190.

[12] Sun F, Fu L, Sun J, Zhang S. A new waste heat district heating system with combined heat and power (CHP) based on ejector heat exchangers and absorption heat pumps. Energy 2014;69:516e24.

[13] Ratlamwala, T.A.H., Dincer, I., 2012. Comparative efficiency assessment of novel multiflash integrated geothermal systems for power and hydrogen production. Appl. Therm. Eng. 48, 359–366.

[14] Onovwiona, H.I., Ugursal, V.I., 2006. Residential cogeneration systems: review ofthe current technology. Renew. Sustain. Energy Rev. 10, 389–431.

[15] M.T. Balta, O. Kizilkan, F. Yılmaz, Energy and exergy analyses of integrated hydrogen production system using high temperature steam electrolysis, Int. J. Hydrogen Energy 41 (2016) 8032e8041.

[16] Ghaebi, Hadi & Farhang, Behzad & Rostamzadeh, Hadi & Parikhani, Towhid. (2017). Energy, exergy, economic and environmental (4E) analysis of using city gate station (CGS) heater waste for power and hydrogen production: A comparative study. International Journal of Hydrogen Energy. 43. 10.1016/j.ijhydene.2017.11.093.

[17] Xinchu Li , Zhongwei Wang . Exergy analysis of integrated TEG and regenerative cooling system for power generation from scramjet heat. Int J Aerospace science and technology 2017:doi;101016/j.ast.2017.02.021.

[18] Huang W. Design exploration of three-dimensional transverse jet in a supersonic crossflow based on data mining and multi-objective design optimization approaches. Int J Hydrogen Energy 2014;39:3914e25.

[19] Bao W, Qin J, Zhou WX, Yu DR. Effect of cooling channel geometry on re-cooled cycle performance for hydrogen fueled scramjet. Int J Hydrogen Energy 2010;35:7002e11.

[20] Choudhuri AR, Gollahalli SR. Combustion characteristics of hydrogen-hydrocarbon hybrid fuels. Int J Hydrogen Energy 2000;25:451e62.

[21] Abdin Z, Webb C.J., Gray E.MacA. modelling and simulation of a proton exchange membrane (PEM) elctrolyzer cell.Int J Hydrogen Energy 40(2015)13243el3257.

[22] Carmo M, fritz DL, Mergel J, Stolen D. A comprehensive review on PEM water electrolysis. Int J Hydrogen Energy 2013;38:4901e34.

[23] Garcia-Valverde R, Espinosa N, Urbina A. Simple PEM water electrolyser model and experimental validation. Int J Hydrogen Energy 2012;37:1927e38.

[24] Lebbal M, Lecauche S. Identification and monitoring of a PEM electrolyser based on dynamical modeling. Int J Hydrogen Energy 2009;34:5992e9.

[25] Leung MKH, Ni M, Leung DYC. Energy and exergy analysis of hydrogen production by a proton exchange membrane (PEM) electrolyzer plant. Energy Convers Manage2008;49:2748e56.

[26] Marangio F, Santarelli M, Calı` M. Theoretical model and experimental analysis of a high pressure PEM water electrolyser for hydrogen production. Int J Hydrogen Energy 2009;34:1143e58.

[27] Ahmadi P, Dincer I, Rosen MA. Energy and exergy analyses of hydrogen production via solar boosted ocean thermal energy conversion and PEM electrolysis. Int J Hydrogen Energy 2013;38:1795e805.
[28] Cengel YA, Boles MA. In: Thermodynamics: an engineering approach. 7th ed. McGraw-Hill; 2011.
[29] Meng NI, Leung MKH, Leung DYC. Energy and exergy analysis of hydrogen production by a proton exchange membrane (PEM) electrolyzer plant. Energy Convers Manage 2008;2008(49):2748e56.
[30] Esmaili P, Dincer I, Naterer GF. Energy and exergy analyses of electrolytic hydrogen production with molybdenum-oxo catalysts. International Journal of Hydrogen Energy 2012;37(9):7365e72.
[31] Ni M, Leung MKH, Leung DYC. Energy and exergy analysis of hydrogen production by a proton exchange membrane (PEM) electrolyzer plant. Energy Convers Manage 2008;49:2748e56.
[32] Nie J, Chen Y, Boehm RF. Numerical modeling of two-phase flow in a bipolar plate of a PEM electrolyzer cell. In: ASME 2008 International mechanical engineering congress and exposition. American Society of Mechanical Engineering; 2008. p. 783e8.
[33] Grigoriev SA, Porembsky VI, Tateev VN. Pure hydrogen production by PEM electrolysis for hydrogen energy. Int J Hydrogen Energy 2006;31:171e5.
[34] The NRC report. The Hydrogen Economy-Opportunites, Costs, Barriers, and R&D Needs 2004 (The National Academies Press, Washington D C)
[35] Bejan, A., Tsataronis, G., and Moran, M. Thermal design and optimization. Jhon Wiley & Sons, (1996), NY, USA.
[36] Kotas, T.J., 2013. The exergy method of thermal plant analysis. Elsevier.